JOM
https://doi.org/10.1007/s11837-021-04704-z

Prediction of Elastic Behavior of Human Trabecular Bone Using A DXA Image-Based Deep Learning Model

PENGWEI XIAO,[1] TINGHE ZHANG,[2] EAKEEN HAQUE,[1] TRENTEN WAHLEN,[1] X. NEIL DONG,[3] YUFEI HUANG,[2,4] and XIAODU WANG [1,5]

1.—Mechanical Engineering, University of Texas at San Antonio, San Antonio, Texas 78249, United States. 2.—Electrical and Computer Engineering, University of Texas at San Antonio, San Antonio, Texas 78249, United States. 3.—Health and Kinesiology, University of Texas at Tyler, Tyler, Texas 75799, United States. 4.—e-mail: yufei.huang@utsa.edu. 5.—e-mail: xiaodu.wang@utsa.edu

Inspired by the recent advancement in deep learning (DL) techniques, this study intended to confirm whether DL models could be trained to predict the elastic behavior of trabecular bone, a highly hierarchical biological material, using its dual-energy x-ray absorptiometry (DXA) images. The convolutional neural network, the most successful DL model in imaging-based predictions, was trained using simulated DXA images of trabecular bone samples as input and their apparent elastic modulus ($E_{apparent}$) determined using microCT-based finite element simulations as output (label). The results showed that the DL model achieved high fidelity in predicting $E_{apparent}$ of trabecular bone samples ($R^2 > 0.86$), and its performance appeared to be better than that of histomorphometric parameter-based regression models built using the same bone samples. The outcome of this study suggests that DXA image-based DL techniques can be used for multiscale modeling of trabecular bone to predict its elastic behavior.

INTRODUCTION

Bone mass loss and adverse microstructural changes at the proximal femur, vertebral body, and wrist bones are the common clinical complications for postmenopausal women and the elderly,[1,2] which may often lead to bone fragility fractures. Current clinical prognosis of bone fragility fractures is dependent mainly on the measurement of bone mineral density (BMD) at the anatomic sites. However, BMD alone could only capture 50%–60% of bone fractures since it is merely a measure of bone mass without considering the microstructural changes of the bone.[3]

To address the issue, investigators have been trying to develop techniques that can account for both bone mass and structural changes to predict the risk of bone fracture accurately.[4–7] Recently, MRI- or CT-based finite element modeling (FEM) techniques have drawn great attention in the field.[8,9] However, due to the limited resolutions, these medical imaging modalities could only capture the shape and 3D density distribution of bone, but not its microstructural features. This drawback has significantly hindered FEM techniques in tackling such multiscale modeling tasks.

In the experimental setting, microCT-based FEM modeling techniques have been very successful in assessing mechanical properties of bone because the resolution of this modality (up to a few micrometers) is sufficient to capture both tissue (material) and microstructural properties of bone. However, this methodology is not suitable for clinical applications because of its high dosage of radiation, which is harmful to patients.

As an alternative, investigators have proposed to use stochastic image processing techniques to capture the textures of dual-energy x-ray absorptiometry (DXA) images since changes in these textures

(Received December 30, 2020; accepted April 19, 2021)

Published online: 19 May 2021

may reflect the variation of bone microstructural features.[10–13] For example, a DXA image texture-based measure, trabecular bone score (TBS), showed a potential in improving DXA prediction of bone fracture risks.[6,14] However, its efficacy in clinical applications is still debated.[15] Indeed, new methodologies are yet to emerge to overcome the limitations to the current technologies.

Recently, deep learning (DL) as a powerful modeling tool has shown great success in biomedical image-based diagnosis/prognosis of diseases, such as skin cancer, Alzheimer disease, and glaucoma.[16–18] These DL models demonstrated great potential in capturing the correlation between the image features and pathological changes in tissue structures, thus significantly improving the accuracy of clinical diagnosis for the diseases. These successes have motivated us to investigate the possibility of using DL to build high-fidelity predictive models that can accurately capture bone mechanical properties simply based on 2D medical images (*i.e.*, DXA). In fact, our previous study has shown that DXA image-based DL models could be trained to predict the microstructural features of trabecular bones.[13]

As a continuing effort, we hypothesize in this study that DXA image-based DL models could accurately predict the elastic behavior of trabecular bone. To test this hypothesis, convolutional neural network (CNN) models were trained and validated to predict the apparent elastic modulus ($E_{apparent}$) of the trabecular bone samples based on their DXA images. The efficacy of the DL models was evaluated against other modeling techniques, *i.e.*, histomorphometric parameter-based regression models.

MATERIALS AND METHODS

Preparation of Trabecular Bone Samples

Six human cadaver proximal femurs were acquired from three female and three male donors. Despite the limited number of donors, the group of samples was considerably diverse in terms of donor genders, ages, and trabecular microstructural parameters (Table I). The proximal femurs were scanned using a microCT system (SkyScan 1173) with a resolution of 35 μm, which had a sufficient resolution to capture the microstructural details of trabecular bone samples.

In this study, 550 trabecular bone cubes (6 mm × 6 mm × 6 mm) were digitally dissected out as representative volume elements (RVEs) from the femoral head, femoral neck, and greater trochanter regions of the six proximal femurs that were reconstructed from microCT scans (Fig. 1). Briefly, trabecular spheres were first dissected out from the proximal femurs (Fig. 1a) and then aligned with the three orthogonal principal axes using a fabric tensor approach as explained below (Fig. 1b). Finally, trabecular cubes inscribed in the trabecular spheres

Table I. General information of trabecular bone samples from human cadaveric proximal femurs (N = 550)

Age (years)	Sex	MicroCT resolution (μm)	No. of cubes	DA	Conn.D (mm^{-3})	BS (mm^2)	SMI	BV/TV	Tb.Th (mm)
22	F	35	90	0.47 ± 0.11	3.42 ± 1.16	690.92 ± 140.41	2.70 ± 0.80	0.41 ± 0.183	0.37 ± 0.14
41	F	35	55	0.55 ± 0.11	3.15 ± 0.76	693.35 ± 105.94	2.56 ± 0.54	0.36 ± 0.12	0.33 ± 0.07
82	F	35	66	0.61 ± 0.09	3.55 ± 0.91	614.78 ± 114.23	3.13 ± 0.46	0.24 ± 0.08	0.26 ± 0.04
24	M	35	204	0.48 ± 0.13	7.52 ± 5.57	725.48 ± 130.67	2.52 ± 0.61	0.36 ± 0.14	0.29 ± 0.08
43	M	35	101	0.45 ± 0.13	6.10 ± 3.77	724.28 ± 122.88	2.49 ± 0.59	0.36 ± 0.12	0.30 ± 0.05
79	M	35	34	0.45 ± 0.09	10.73 ± 4.92	813.48 ± 58.54	2.33 ± 0.37	0.55 ± 0.15	0.40 ± 0.12

Note The parameters are presented as mean ± SD.

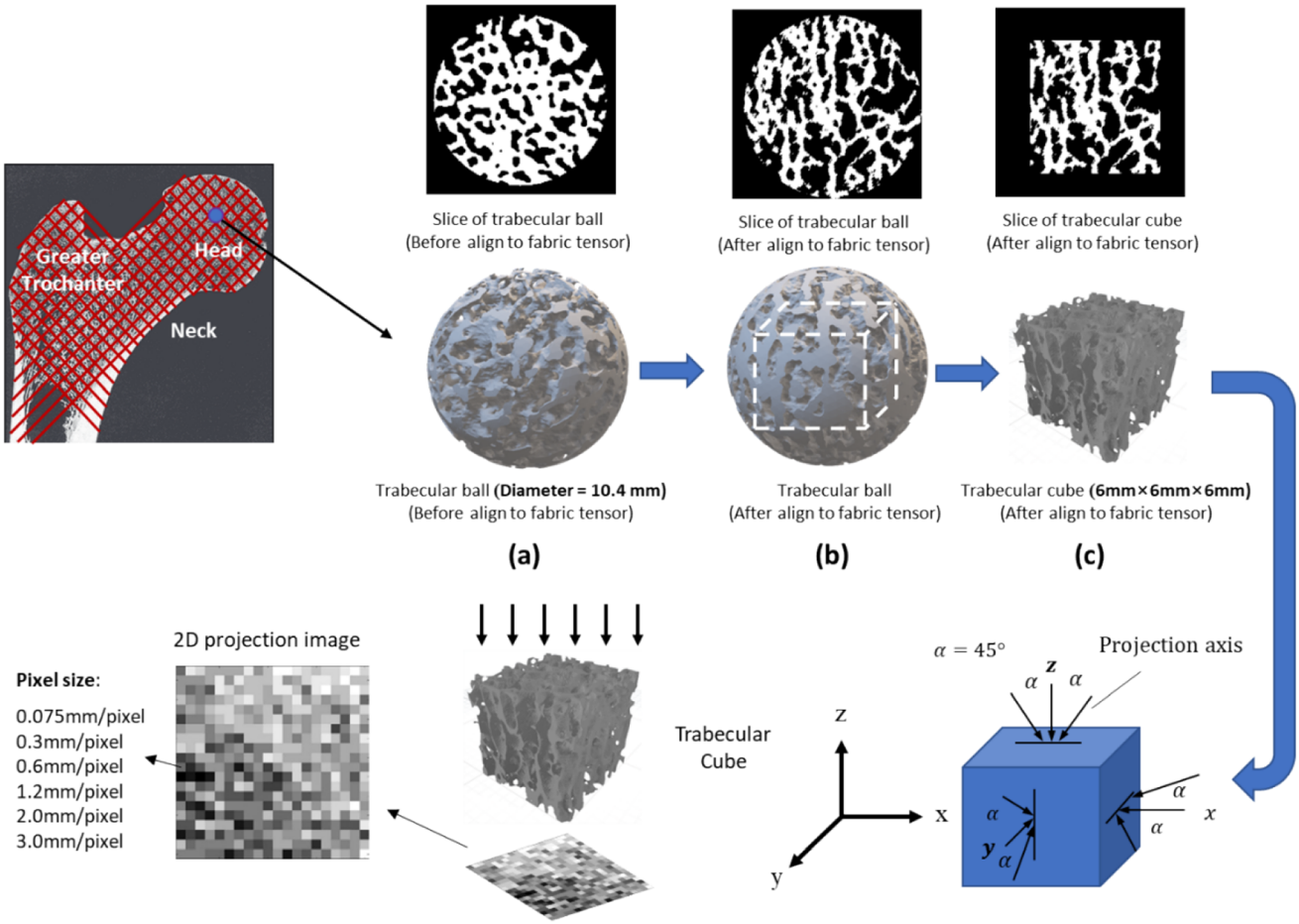

Fig. 1. Schematic representation of methods for preparing trabecular bone cubes (6 mm × 6 mm × 6 mm) from the femoral head, neck, and greater trochanter regions and acquisition of simulated DXA images from the cubes. The projection directions were designated in x, y, z, x ± 45°, y ± 45°, and z ± 45°. The pixel size of the simulated DXA images varied from 0.075 mm to 3.0 mm/pixel by changing the bin size for the projections.

were dissected out, with its edges aligned with the three principal axes (Fig. 1c).

Aligning Trabecular Bone Cubes with Three Orthogonal Principal Directions

Trabecular bone is an orthotropic material exhibiting symmetry about three orthogonal principal directions. Thus, the elastic behavior of trabecular bone varies with the loading directions. To determine the effect of trabecular bone anisotropy on the prediction of apparent elastic modulus, all trabecular bone cubes were aligned with the three orthogonal principal axes before taking DXA images and determining their apparent elastic modulus.

The microstructural anisotropy of trabecular bone can be quantified by a fabric tensor, which is a second-rank positive definite tensor and is commonly computed using the mean intercept length (MIL) image analysis method.[19] The principle of the MIL method is to count the number of intersections between a linear grid and bone tissue surfaces in a cross-sectional plane as the linear grid rotating in 3D orientations.[20] The relationship between the mean intercept length L and the fabric tensor is given as follows:[19]

$$1/L^2 = \boldsymbol{n}[\boldsymbol{M}]\boldsymbol{n} \quad (1)$$

where $[\boldsymbol{M}]$ is a second-rank fabric tensor, L is the mean intercept length, and $\boldsymbol{n}$ is a unit vector representing the normal of the plane, in which L was measured. The three eigenvectors of a fabric tensor represent the three principal axes of anisotropy, while the three associated eigenvalues represent the magnitude of anisotropy along the corresponding three principal axes, respectively.

The fabric tensor was determined for each trabecular sphere, and the three orthogonal principal directions were calculated using ImageJ (1.52 h).

Then, the trabecular sphere was rotated to align with the three orthogonal principal directions. Finally, trabecular cubes (6 mm × 6 mm × 6 mm) were dissected out from the aligned trabecular spheres, with their edges aligned with the corresponding principal directions (Fig. 1).

Measurement of the Apparent Elastic Modulus ($E_{apparent}$) using FEM Simulations

Finite element modeling (FEM) was employed to assess the apparent elastic modulus ($E_{apparent}$) of each trabecular cube in its three principal axes, respectively, with these values used as labels (output) for training the DL models. First, the trabecular cubes were digitally reconstructed in STL format from the microCT scans. Then, the digitized trabecular cubes were imported into the commercial FEM software ABAQUS 2017/Standard software package and were converted to FEM models using first-order tetrahedral elements (C3D4). For each model, approximately 0.5 to 2.5 million tetrahedral elements were generated. Multiple-step static simulations of compression tests were implemented using the FEM models to assess $E_{apparent}$ of the trabecular bone cubes. Two rigid plates were modeled at the top and bottom of the trabecular cubes to ensure a uniform loading condition. Contact elements (node to surface contact) with a friction coefficient of 0.2[21] for tangential behavior and "hard" contact for normal behavior were used to define proper contacts between the rigid plates and the trabecular cube. To capture the elastic to plastic transition, an isotropic linear elastic perfectly plastic material model was used in the FE model, with a yield stress of 120 MPa.[22] The material properties at the tissue level were assumed to be homogeneous and isotropic, with Young's modulus being 15 GPa and Poisson's ratio being 0.3.[23] $E_{apparent}$ was assessed in the linear part of the force-displacement curve using the following formula:

$$E_{apparent} = FL/(A\Delta) \tag{2}$$

where F is the applied force on the trabecular cube model, L is the height of the trabecular cube in the loading direction, A is the cross-section area of the trabecular cube, and Δ is the displacement in the loading direction. In each compression test, a uniaxial displacement equaling 8.3% of the height of the trabecular bone cubes (0.5 mm) was applied perpendicularly to the upper surface of trabecular bone cubes *via* the rigid plate, with its lower surface fixed in the loading direction and free in other two directions. The simulation was implemented in multiple displacement steps to obtain the force-displacement curve. All the simulated compression tests were performed on Desktop computers [XPS Desktop Special Edition, 10th Gen Intel Core i9-10900K processor (20 logical processors), 128 GB memory, 2 TB M.2 PCIe NVME SSD + 2 TB SATA 7200 RPM HDD], and about 1–3 h was required to complete each compression test depending on the size of the FEM model elements.

To assess the capability of DL models to capture the effect of anisotropy, $E_{apparent}$ in all three principal axes was determined using the aforementioned FEM simulations, respectively.

Simulated DXA Image

In this study, DXA images were not obtained from experimental measurements, but from *in silico* simulations. Our previous studies[12,24] as well as the literature[25–27] confirmed that the simulated DXA images are representative of the real DXA images obtained from the proximal femur.[25] Simulated DXA images were digitally generated for each trabecular bone cube by projecting the 3D model of the cube onto planes perpendicular to a set of designated projection directions. Briefly, voxelization was first performed to convert the 3D geometric model of each trabecular bone cube, which is in STL format, to a 3D voxel-based model that best approximated the geometric model.[28] The voxel-based model was then dissected into a stack of plane layers, with each layer being represented by an array of voxels. Next, the simulated DXA image of each cube was generated by summing the binarized values in each pixel in the projection plane according to a designated resolution (Fig. 1). In this plane, the greyscale value (Z) of the pixel at the location (x, y) was determined by the following equation[11]:

$$Z(x,y) = \frac{1}{N}\sum_{i=1}^{N} V(x,y,z) \tag{3}$$

where $Z(x, y)$ represents the grayscale value in each pixel of the simulated DXA image at the location (x, y), $V(x, y, z)$ is the binarized value of each voxel at the location (x, y, z), and N is the number of stacks of image layers in the projection direction.

To investigate the effect of the resolution of simulated DXA images on the prediction accuracy of the DL models, six different resolutions of simulated DXA images were generated from coarse to fine 3D voxel models of the trabecular bone cubes by meshing the cube using different numbers of voxels. The resolutions used in this study were 3.0 mm (2 × 2 × 2 voxels), 2.0 mm (3 × 3 × 3 voxels), 1.2 mm (5 × 5 × 5 voxels), 0.6 mm (10 × 10 × 10 voxels), 0.3 mm (20 × 20 × 20 voxels), and 0.075 mm (80 × 80 × 80 voxels), respectively.

This study also intended to investigate the effect of the number of simulated DXA images on the prediction accuracy of the DL models. Nine projection directions, including the x, y, and z axis and ± 45° about the three axes, were used to generate simulated DXA images. The simulated DXA images were grouped as a single projection (along the x-, y-, or z-axis), a triple-projection (along the x-, y-, and z-axis),

a sextuple-projection (along x, y, and z, x + 45°, y + 45°, and z + 45°), or nonuple-projection directions (along x, y, z, x ± 45°, y ± 45°, and z ± 45°) (Fig. 1).

Convolutional Neural Network (CNN) Modeling

A popular DL model called the convolutional neural network (CNN)[29] was used in this study because CNN is the most successful DL model in imaging-based predictions. Two DL models were developed in this study: one was trained to predict the elastic behavior of trabecular bone cubes in a designated principal direction (*i.e.*, the first principal axis), and the other was trained to predict the elastic behavior of trabecular bone cubes in randomly chosen principal directions.

The architecture and parameters of the proposed CNN models are shown in Fig. 2 and Table II. The CNN model was programmed in Python using Keras library with a TensorFlow backend and was trained on a Dell desktop computer (XPS 8930, Intel Core i9-9900k 8-Core Processor, 64 GB Memory, NVIDIA® GeForce(R) GTX 1080 with 8 GB GDDR5X Graphic Memory). The input for the CNN model was simulated DXA images of the trabecular bone cubes and the output (label) was $E_{apparent}$ either in a designated direction (*i.e.,* the first principal axis) or in a direction randomly chosen from the three principal axes (Table II). Thus, two CNN models were trained in this study: one was to predict $E_{apparent}$ in a designated principal direction and the other was to predict $E_{apparent}$ in a randomly chosen principal direction.

The CNN model of this study comprised three convolutional layers, three max-pooling layers, and one fully connected neural network layer with 64 neurons, followed by the output layer. In this model, we used unpadded 3 × 3 convolutions and 2 × 2 max-pooling with stride 1 to decrease the dimension of the feature maps while maintaining the most important features. During the training process, the simulated DXA images were used as the input, and the apparent elastic moduli in the three principal axes were used as output (label). The mean square error (MSE) was employed as the loss function, defined as

$$MSE = \frac{1}{2}\sum_{i=i}^{n}(y_i - \hat{y}_i)^2 \quad (4)$$

where y_i is the measured histomorphometric parameter and $\hat{y}_i$ is the predicted parameter, and n is the total number of samples (or sample size). The stochastic gradient algorithm with the ADAM optimizer was used to train the CNN models. Moreover, hyperparameter optimization was performed to tune the architecture of the CNN model for the optimal performance. The evaluated parameters of CNN architecture included the number of convolutional layers, the number of fully connected layers, the number of filters and kernel size, the optimizer functions, the learning rates, the number of epochs, and the value of dropout. In the end, the best parameters for the architecture of the CNN model were finalized.

Since $E_{apparent}$ of trabecular bone cubes was not normally distributed, normalization was performed to rescale the data before training the CNN models. In this study, minimum-maximum normalization was used because our pilot study indicated that it was slightly more accurate than other scaling methods. Rescaling is an efficient method for normalizing the data and scales the range of trained features in [0, 1]. In addition, the rescaling keeps the relationship among the original data, which works well for the predictive model. The rescaling was calculated by the following formula:

$$x' = \frac{x - min(x)}{max(x) - min(x)} \quad (5)$$

where x is an original value, and x' is the normalized value.

The performance of the CNN models was verified by using the cross-validation approach during the training process. Eighty percent of the simulated DXA images and the associated apparent elastic modulus were randomly selected from the entire dataset (N = 550) as the training data. Of the training data, 80% were randomly selected to train the CNN model, and the other 20% of data were used to modify the parameters of the CNN model to optimize its performance in predicting $E_{apparent}$ of

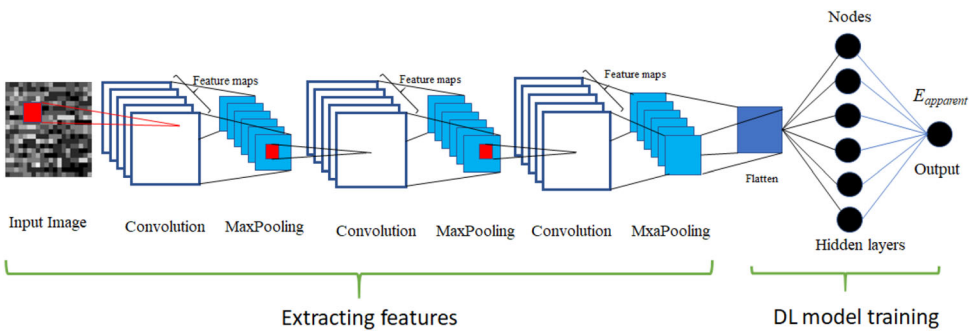

Fig. 2. Schematic architecture of the CNN model used for prediction of $E_{apparent}$ of trabecula bone cubes using DXA images as input.

Table II. Architectural features/parameters of the CNN models for predicting apparent elastic modulus

Model	Input	Kernel size	Pool size	Convolutional layers	No. of hidden layers	Learning rates	Number of epochs	Number of filters	Dropout	Label
1	Simulated DXA images	3 × 3	2 × 2	(8,16,32)	1	0.0001	250	64	0.3	$E_{apparent}$ in designated direction
2	Same as above	3 × 3	2 × 2	(8,16,32)	1	0.0001	250	64	0.3	$E_{apparent}$ in random directions

trabecular bone cubes. The remaining 20% of the whole dataset was used to evaluate the DL models.

Evaluation of DL Model Performance

Comparison Between DL and MicroCT-Based FEM Models

First, the two DXA image-based DL models trained using the training dataset (80% of the whole dataset) were employed to predict $E_{apparent}$ of the trabecular bone cubes from the testing dataset (20% of the whole dataset). Then, the values of $E_{apparent}$ predicted by the DL models were compared with those (*i.e.*, the labels) obtained from the microCT-based FEM simulations using the same bone samples. The squared correlation coefficient (R^2) between the $E_{apparent}$ values predicted by the DL models and those determined by the FEM simulations was calculated in IBM SPSS Statistics software (version 25), and used as the measure to assess the prediction accuracy of the DL models.

Comparison Between DL and Multiple Regression Models

The prediction accuracy (R^2) of the DL models was also compared against that of multiple regression models, in which the histomorphometric parameters were used as the independent variables and $E_{apparent}$ as the dependent variable to evaluate the performance of the DL models. Indeed, such multiple regression models have been shown to be reasonably accurate in predicting the elastic behavior of trabecular bone samples.[30] Similar to training the DL models, the training dataset (80% of the whole sample population) was used to develop the multiple regression models, whereas the testing dataset (the remaining 20% bone samples) was employed to determine the accuracy (R^2) of the regression models in predicting $E_{apparent}$ in both the designated principal axis and the randomly chosen principal axes.

Six major histomorphometric parameters were used to build the regression models, which included the degree of anisotropy (DA), connectivity density (Conn.D), bone surface (BS), structure model index (SMI), bone volume fraction (BV/TV), and trabecular thickness (Tb.Th) (Table I). Among the parameters, BV/TV is directly related to BMD, Tb.Th defines the average thickness of trabeculae, BS is a measure of bone surface area, Conn.D is the trabecular connectivity density pertaining to the trabecular number per unit volume, SMI defines whether the trabecular bone structure is either plate-like or rod-like, and DA measures the anisotropy of the trabecular bone. These histomorphometric parameters were measured using Image-J (NIH biomedical image processing software) for each trabecular bone cube in the whole dataset (Table I).

The stepwise multiple regression method was utilized to develop the multiple regression models with all six histomorphometric parameters. At each step of regression, independent variables with the highest statistical strength stayed in the model, whereas the variables with the least statistical strength were removed from the model. The stepping was terminated when no eligible independent variable exceeded the critical value ($p < 0.5$) for model entry or when no independent variable in the model reached the standard ($p > 0.1$) for variable removal.

Comparison Between DL and BV/TV-Based Regression Models

In clinical applications, bone mineral density (BMD) has been commonly used to predict the risk of bone fractures. Since BV/TV is representative of BMD, a linear regression model ($E_{apparent}$ = a (BV/TV) + b) and two non-linear regressions models, *i.e.*, Yang's model ($E_{apparent} = E_{tissue}$ 1240 $(BV/TV)^{1.8}$)[31] and Kabel's model ($E_{apparent} = E_{tissue}$ 813 $(BV/TV)^{1.93}$),[32] were also used to evaluate the performance of the DL models. In these regression models, BV/TV was used as the sole independent variable and a constant value was assumed for E_{tissue} (15GPa), which represents the tissue elastic modulus of trabecular bone. Similarly, the training dataset was used to develop the linear regression model, whereas the testing dataset was used to determine its prediction accuracy. Since the two non-linear regression models are fully developed empirical models, only the testing dataset was needed to determine the prediction accuracy of the models.

RESULTS

Prediction Accuracy of the DL Models

$E_{apparent}$ of trabecular bone cubes predicted by the DXA image-based DL models indicated a strong correction with those assessed using FEM simulations in both the designated principal direction (R^2 = 0.872) and the randomly chosen principal directions (R^2 = 0.861), with the p-values being < 0.0001 (Fig. 3a and b). Using R^2 values as the measure of prediction accuracy of DL models, these results showed that the DL models had reasonably high accuracy in predicting $E_{apparent}$ irrespective of the orientation-dependence of the trabecular bone elastic behavior, thus suggesting that the DL model could capture the anisotropic elastic behavior of trabecular bone.

It was also noted that the DL model had much better prediction accuracy for the trabecular bone cubes with $E_{apparent}$ < 6.0 GPa, whereas large deviations appeared in the DL model predicted values compared to those obtained from the FEM simulations when $E_{apparent}$ > 6.0 GPa (Fig. 3). This might be attributed to the fact that there were a few samples with $E_{apparent}$ > 6.0 GPa, thus significantly diminishing the prediction accuracy of the DL models in that region.

The Effect of the Resolution and Number of DXA Images on the Prediction Accuracy

The prediction accuracy of the DL models improved considerably with increasing image resolutions in predicting $E_{apparent}$ of trabecular bone cubes in both the designated principal direction and the randomly chosen principal directions (Fig. 4a). However, the prediction accuracy leveled off as the image resolution approached 0.6 mm/pixel and kept almost constant after 0.3 mm/pixel. This observation suggests that the image resolution of the current DXA techniques (up to 0.3 mm/pixel) is sufficient for the DL models to predict $E_{apparent}$ of trabecular bone cubes accurately.

In addition, the prediction accuracy of the DL model improved considerably as the number of simulated DXA images increased (Fig. 4b) to predict $E_{apparent}$ of trabecular bone cubes in both the designated principal direction and the randomly chosen directions. However, the prediction accuracy leveled off as the input DXA image number was > 3. This implies that at least three projections of DXA might be required to train a high-fidelity DL model in predicting $E_{apparent}$ of trabecular bone.

Regression Models Using BV/TV as the Sole Independent Variable

Both the linear and non-linear regression models using BV/TV as the sole independent variable demonstrated similar accuracies in predicting $E_{apparent}$ in the designated principal direction (R^2 = 0.840–0.881) and in the randomly chosen principal directions (R^2 = 0.715–0.770) (Table III). The results indicated that these regression models were insensitive to the variance of $E_{apparent}$ of trabecular bone cubes in different orientations.

Multiple Linear Regression Model Using all Six Histomorphometric Parameters

The multiple linear regression model using the aforementioned six microstructural parameters had high accuracy in predicting $E_{apparent}$ in the designated principal direction (R^2 = 0.867). However, the prediction accuracy significantly decreased in predicting $E_{apparent}$ in the randomly chosen principal directions (R^2 = 0.752). In addition, the results from the stepwise regression indicated that BV/TV was the most important predictor of $E_{apparent}$ for both the cases, with BS and SMI as secondary predictors (Table III).

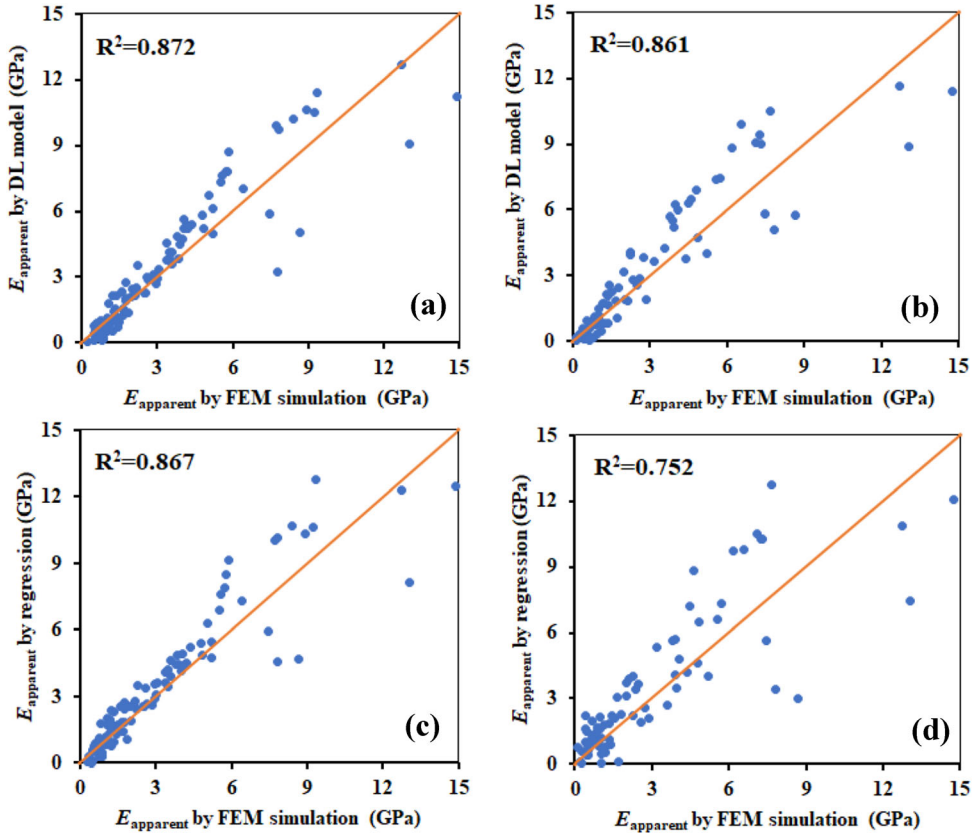

Fig. 3. Regression plots of $E_{apparent}$ predicted by the DL model vs. microCT-based FEM model in the designated direction (a) and in random directions (b) and by the multiple regression model vs. microCT-based FEM model in the designated direction (c) and in random directions (d).

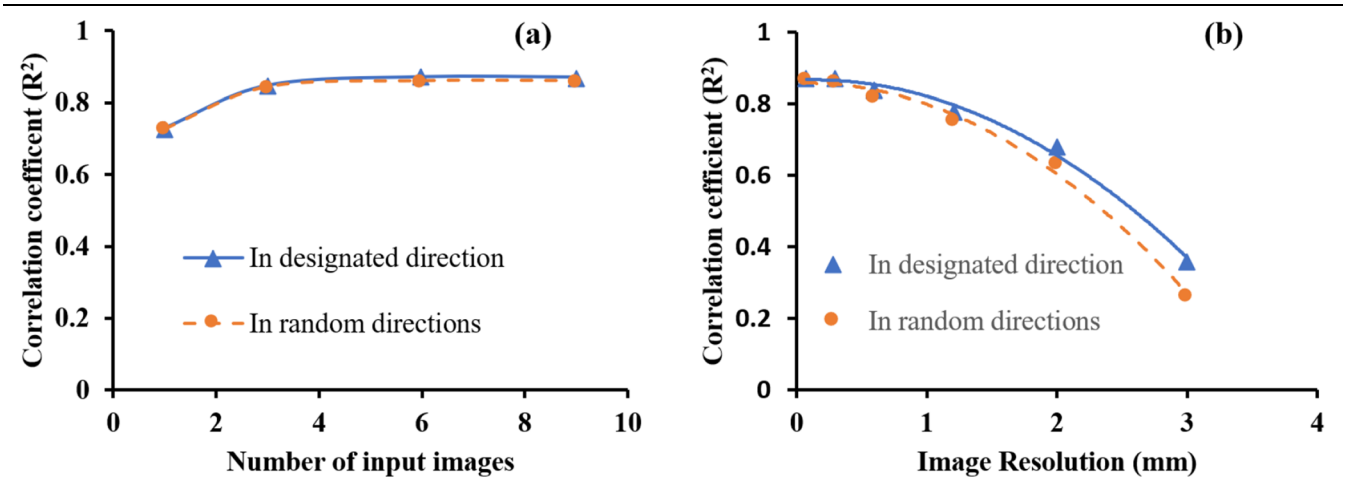

Fig. 4. Effect of the number (a) and resolution (b) of simulated DXA images on the prediction accuracy of the DL models to predict $E_{apparent}$ in both the designated and randomly chosen principal direction. Nine projections of DXA images were used in (a), and 0.3 mm/pixel was used as DXA image resolution in (b).

Comparison Between the DL Models and Regression Models

The prediction accuracy (R^2) in accessing $E_{apparent}$ of trabecular bone cubes was calculated for the DL models and all BV/TV-based regression models, respectively, and is illustrated in Table III. The results indicated that the DL models had similar accuracy in predicting $E_{apparent}$ irrespective of the loading directions (in either the designated principal direction or the randomly chosen directions), suggesting that the DL model was able to capture

Table III. Prediction accuracy (R^2) of the DL and all regression models

	Prediction accuracy (R^2)				
			BV/TV as the sole independent variable		
Predicted property	DL	Multiple step-wise regression	Linear regression	Yang's model	Kabel's model
$E_{apparent}$ in a designated direction	0.872	0.867	0.840	0.872	0.881
$E_{apparent}$ in random directions	0.861	0.752	0.715	0.766	0.770

the orientation dependence of $E_{apparent}$ of the trabecular bone samples. However, all the regression models appeared to have much less accuracy (R^2 = 0.715–0.770) in predicting $E_{apparent}$ in the randomly chosen principal directions, although their prediction accuracies were comparable with that of the DL model in predicting $E_{apparent}$ in the designated principle direction (R^2 = 0.84–0.881).

DISCUSSION

This study investigated the feasibility of using DXA image-based DL modeling techniques to predict $E_{apparent}$ of trabecular bone samples. The results indicated that the DL models trained using the simulated DXA images had a reasonably high fidelity (R^2 = 0.861–0.872) in predicting $E_{apparent}$ of trabecular bone samples, thus supporting the hypothesis of this study. More importantly, this is the first attempt ever to use a non-conventional methodology for multiscale modeling of trabecular bone, a complex and highly hierarchical biological material. It is worth mentioning that DL modeling does not provide an explicit formulation that relates the material and microstructural properties of trabecular bone to its elastic behavior, but a DXA image-based convolutional neural network (CNN) with all underlying mechanisms unknown, but hidden in the model.

This study was a continuation of our previous study, which showed that a full set of microstructural features of trabecular bone (*e.g.*, DA, SMI, BV/TV, Tb.Th, Conn.D, and BS) could be captured by DXA image-based DL models.[13] Since the elastic behavior of trabecular bone is highly correlated with its microstructural features,[33,34] it could be reasonably conjectured that DXA image-based DL models are also capable of predicting the elastic behavior of trabecular bone. Indeed, the results of this study have proved the speculation. The DXA image-based DL models trained in this study showed reasonably high prediction accuracies (R^2 = 0.861–0.872) in predicting $E_{apparent}$ of trabecular bone, whereas the regression models obtained from the histomorphometric parameters exhibited lower prediction accuracies in a range of R^2 = 0.715–0.881 (Table III). The results indicated that the DXA image-based DL models are more accurate in predicting trabecular bone's elastic modulus than the regression model using the microstructural variables, thus suggesting that the trained CNN models could also capture additional features specific to elastic behavior besides those microstructural features.

One important observation of this study is that increasing the DXA image resolution could markedly improve the prediction accuracy of the DL models if the image resolution reaches beyond 0.3 mm/pixel (Fig. 4). Since the resolution of clinical DXA images is usually around 1.0 mm/pixel and could be up to 0.3 mm/pixel,[35] this observation suggests that high-resolution DXA images could ensure that the DL models predict the elastic behavior of trabecular bone with a reasonably high accuracy. This finding provides convincing evidence that, assisted by DL techniques, DXA (the most accessible and affordable imaging modality in clinical applications) has great potential for clinical prognosis of osteoporotic bone fractures.

In addition, the number of input DXA images may also have a remarkable effect on the accuracy of DL models in predicting the elastic behavior of trabecular bone (Fig. 4). It is not surprising because from the computer graphics perspective, use of DXA images projected from different directions could provide more information on the spatial characteristics of the trabecular microstructure, thus making it easier for the DL model to capture and subsequently to relate the features to the elastic behavior of trabecular bone. This information is also important for future development of advanced DXA techniques for the clinical prognosis of bone fracture risks.

Another important finding of this study is that the DL models are capable of capturing the orientation-dependent elastic behavior of trabecular bone, showing that its prediction accuracy is not affected (R^2 = 0.861–0.872) when predicting the elastic behavior in different orientations even using the same input DXA images (Fig. 3 and Table III). Previous studies have demonstrated that the difference in elastic modulus could be as large as 53% among the trabecular bone samples having the same BV/TV.[36] Thus, BV/TV alone is not a reliable predictor of the elastic behavior of trabecular bone.

This is consistent with the observation of this study that the regression models with BV/TV as the sole independent variable were not sensitive to catching the variance of the elastic behavior of trabecular bone in different directions (Table III). In addition, it is noteworthy that the multiple regression model, which even included an anisotropy-related parameter (DA), failed to capture the variance of the elastic modulus in different orientations (Fig. 3 and Table III). This is largely because DA is only a descriptive measure of overall anisotropic feature rather than the orientation dependence of the trabecular bone's elastic behavior.

Previous studies have used a fabric tensor to account for the anisotropy in determining the elastic behavior of trabecular bones.[37–42] Kabel et al.[42] conducted a study to define the relationships between the elastic behavior and volume-based fabric tensor using microCT image-based μFE models, showing that the proposed model could accurately predict the elastic stiffness of trabecular bone with a correlation coefficient of $R^2 > 0.93$. This suggests that microstructural anisotropy must be considered in building predictive models to predict the elastic behavior of trabecular bone accurately. The results of this study demonstrate that even low-resolution DXA image-based DL models are able to catch the orientation-dependent variance in the elastic behavior of trabecular bone samples. A possible explanation is that DXA images, even though very coarse, contain sufficient orientation-dependent features of trabecular bone microstructures, thus enabling the DL models to be comparable to high-resolution μFE models for accurate prediction of the elastic behavior of trabecular bone irrespective of its orientations.

There are several limitations of this study. First, the DL models developed in this study do not give rise to inherent relationships between the material and structural properties and the mechanical behavior of trabecular bone. Second, the sample population was limited to only six donors in this study. Although different ages and genders are included, this small donor population is not necessarily representative of the entire human population. Nonetheless, this sample population covers a large variety of trabecular bone microstructures and thus is suitable for testing the hypothesis of this study. Third, trabecular bone tissue properties were assumed to be constant and homogeneous, which may not be fully representative of real bone. Finally, the input data (*i.e.*, simulated DXA images) used in this study for training the DL models were not acquired from the real DXA measurements, but *via* computational simulations. Nonetheless, previous studies have shown that the simulated DXA images are comparable to real DXA images. Finally, this study focused only on the elastic behavior of trabecular bone. In fact, DL modeling techniques may also be used to predict stress-strain curves of human trabecular bone from DXA images.[43,44] This would be an interesting and important research topic for future studies.

CONCLUSION

This study indicates that DXA image-based DL models could be used to predict the elastic behavior of trabecular bone with reasonably high accuracies. The other important findings of this study include: (1) The DL models appear to be able to capture the anisotropic elastic behavior of trabecular bone. (2) The minimum DXA image resolution required for training a high-fidelity DL model has to be better than 0.6 mm/pixel. (3) DXA images in at least three orthogonal projections are required to ensure the maximum accuracy in predicting the elastic behavior of trabecular bone. The outcome of this study could be used to help develop DXA image-based DL techniques for clinical assessment of bone quality, thus ensuring accurate prognosis of bone fracture risks.

ACKNOWLEDGEMENTS

The authors are grateful to Mr. James Schmitz at UT Health San Antonio for technical assistance in the acquisition of microCT scans of human cadaveric proximal femur samples.

CONFLICT OF INTEREST

On behalf of all authors, the corresponding author states that there is no conflict of interest.

REFERENCES

1. N.C. Wright, A.C. Looker, K.G. Saag, J.R. Curtis, E.S. Delzell, S. Randall, and B. Dawson-Hughes, *J. Bone Miner. Res.* 29, 2520. (2014).
2. R. Bouillon, P. Burckhardt, C. Christiansen, H. Fleisch, T. Fujita, C. Gennari, T. Marin, G. Mazzuoli, L. Melton, and J. Ringe, *Am. J. Med.* 90, 107. (1991).
3. E.S. Siris, Y.T. Chen, T.A. Abbott, E. Barrett-Connor, P.D. Miller, L.E. Wehren, and M.L. Berger, *Arch. Intern. Med.* 164, 1108. (2004).
4. H.K. Genant, K. Engelke, T. Fuerst, C.C. Glüer, S. Grampp, S.T. Harris, M. Jergas, T. Lang, Y. Lu, and S. Majumdar, *J. Bone Miner. Res.* 11, 707. (1996).
5. L. Pothuaud, P. Carceller, and D. Hans, *Bone* 42, 775. (2008).
6. R. Winzenrieth, A. Heraud, B. Rabier, P. Carceller, L. Pothuaud, and D. Hans, *Calcif. Tissue Int.* 82, S181. (2008).
7. G.L. Niebur, M.J. Feldstein, J.C. Yuen, T.J. Chen, and T.M. Keaveny, *J. Biomech.* 33, 1575. (2000).
8. B. Borah, G.J. Gross, T.E. Dufresne, T.S. Smith, M.D. Cockman, P.A. Chmielewski, M.W. Lundy, J.R. Hartke, and E.W. Sod, *Anat. Rec. Off. Publ. Am. Assoc. Anat.* 265, 101. (2001).
9. M. Bessho, I. Ohnishi, H. Okazaki, W. Sato, H. Kominami, S. Matsunaga, and K. Nakamura, *J. Orthop. Sci.* 9, 545. (2004).
10. T. Le Corroller, J. Halgrin, M. Pithioux, D. Guenoun, P. Chabrand, and P. Champsaur, *Osteoporos. Int.* 23, 163. (2012).
11. X.L.N. Dong, M. Shirvaikar, and X.D. Wang, *Bone* 56, 327. (2013).
12. X.N. Dong, R. Pinninti, A. Tvinnereim, T. Lowe, D. Di Paolo, and M. Shirvaikar, *J. Biomech.* 48, 2968. (2015).

13. P. Xiao, T. Zhang, X.N. Dong, Y. Han, Y. Huang, and X. Wang, *Bone Rep.* 13, 100295. (2020).
14. A.W. Popp, S. Meer, M.A. Krieg, R. Perrelet, D. Hans, and K. Lippuner, *Eur. Spine J.* 25, 3432. (2016).
15. L. Pothuaud, N. Barthe, B. Merino, P. Carceller, and D. Hans, *Bone* 40, S248. (2007).
16. A. Esteva, B. Kuprel, R.A. Novoa, J. Ko, S.M. Swetter, H.M. Blau, and S. Thrun, *Nature* 542, 115. (2017).
17. Y. Ding, J.H. Sohn, M.G. Kawczynski, H. Trivedi, R. Harnish, N.W. Jenkins, D. Lituiev, T.P. Copeland, M.S. Aboian, and C.M. Aparici, *Radiology* 290, 456. (2019).
18. X.Y. Chen, Y.W. Xu, S.C. Yan, D.W.K. Wong, T.Y. Wong, and J. Liu, *Medical Image Computing and Computer-Assisted Intervention, Pt Iii*. 9351, 669 (2015).
19. T. Harrigan, and R. Mann, *J. Mater. Sci.* 19, 761. (1984).
20. A. Odgaard, *Bone* 21, 191. (1997).
21. M.S. Hefzy, and S.P. Singh, *Med. Eng. Phys.* 19, 50. (1997).
22. H.J. Leng, X.N. Dong, and X.D. Wang, *J. Biomech.* 42, 491. (2009).
23. S.A. Goldstein, *J. Biomech.* 20, 1055. (1987).
24. X.N. Dong, Y. Lu, M. Krause, G. Huber, Y. Chevalier, H. Leng, and G. Maquer, *J.. Biomech.* 77, 223. (2018).
25. B.C. Khoo, K. Brown, C. Cann, K. Zhu, S. Henzell, V. Low, S. Gustafsson, R.I. Price, and R.L. Prince, *Osteoporos. Int.* 20, 1539. (2009).
26. A.J. Burghardt, G.J. Kazakia, T.M. Link, and S. Majumdar, *Osteoporos. Int.* 20, 2017. (2009).
27. E. Dall'Ara, D. Pahr, P. Varga, F. Kainberger, and P. Zysset, *Osteoporos. Int.* 23, 563. (2012).
28. S. Patil and B. Ravi, *International Conference on Computer Aided Design and Computer Graphics* 415 (2005).
29. H. Kandi, D. Mishra, and S.R.K.S. Gorthi, *Comput Secur.* 65, 247. (2017).
30. X.S. Liu, X.H. Zhang, K.K. Sekhon, M.F. Adams, D.J. McMahon, J.P. Bilezikian, E. Shane, and X.E. Guo, *J. Bone Miner. Res.* 25, 746. (2010).
31. G.Y. Yang, J. Kabel, B. Van Rietbergen, A. Odgaard, R. Huiskes, and S.C. Cowin, *J. Elast.* 53, 125. (1998).
32. J. Kabel, A. Odgaard, B. van Rietbergen, and R. Huiskes, *Bone* 24, 115. (1999).
33. E. Mittra, C. Rubin, B. Gruber, and Y.-X. Qin, *J. Biomech.* 41, 368. (2008).
34. B. Helgason, E. Perilli, E. Schileo, F. Taddei, S. Brynjolfsson, and M. Viceconti, *Clin. Biomech.* 23, 135. (2008).
35. V. Boudousq, D.M. Goulart, J.M. Dinten, C.C. de Kerleau, E. Thomas, O. Mares, and P.O. Kotzki, *Osteoporos. Int.* 16, 813. (2005).
36. D. Ulrich, B. Van Rietbergen, A. Laib, and P. Ruegsegger, *Bone* 25, 55. (1999).
37. S.C. Cowin, *Mech. Mater.* 4, 137. (1985).
38. M. Moesen, L. Cardoso, and S.C. Cowin, *Mech. Mater.* 54, 70. (2012).
39. R. Moreno, O. Smedby, and D.H. Pahr, *Biomech. Model. Mechanobiol.* 15, 831. (2016).
40. B. Van Rietbergen, A. Odgaard, J. Kabel, and R. Huiskes, *J. Orthopaed. Res.* 16, 23. (1998).
41. C.H. Turner, S.C. Cowin, J.Y. Rho, R.B. Ashman, and J.C. Rice, *J. Biomech.* 23, 549. (1990).
42. J. Kabel, B. van Rietbergen, A. Odgaard, and R. Huiskes, *Bone* 25, 481. (1999).
43. C. Yang, Y. Kim, S. Ryu, and G.X. Gu, *Mater. Design.* 189, 108509. (2020).
44. C. Yang, Y. Kim, S. Ryu, and G.X. Gu, *MRS Commun.* 9, 609. (2019).